Electronic Supplementary Material (ESI) for ChemComm.

Strain engineering improves the photovoltaic performance of carbon-based hole-transport-material free $CsPbIBr_2$ perovskite solar cells

Wei He,[#a] Xingxing Duan,[#b] Qunwei Tang,[b] Jie Dou*[b] and Jialong Duan *[b]

Materials and reagents

Unless special instructions, all materials and reagents were purchased from commercial suppliers and used as received without further purification. Cesium iodide (CsI, 99.9 %) and dimethylsulfoxide (DMSO, 99.7 %) were purchased from Aladdin Chemistry Co. Ltd. (Shanghai, China). Lead iodide (PbI_2, >99.99 %) was purchased from Xi'an Polymer Light Technology Corp. (Xi'an, China). Lead bromide ($PbBr_2$, 99.0 %) was obtained from Macklin reagent Co. Ltd. (Shanghai, China). The low-temperature carbon paste (99.0 %) was purchased from Shanghai MaterWin New Materials Co., Ltd. N-Butylamine ($C_4H_{11}N$,>99%) purchased from Macklin reagent Co., Ltd. (Shanghai, China). N-Hexanamine ($C_6H_{15}N$,>99%) purchased from Mindray Biochemical Technology Co., Ltd. (Shanghai, China). N-Octylamine ($C_8H_{19}N$, >99%) purchased from Aladdin Chemical Co., Ltd. (Shanghai, China).

Fabrication of solar cells

The fluorine-doped tin dioxide (FTO) coated glass with desired pattern was firstly etched with zinc powder and HCl, and then thoroughly washed in detergent, acetone, isopropanol and deionized water. Prior to fabrication of solar cells, the cleaned FTO substrate was treated with plasma for 180 s and a compact TiO_2 (c-TiO_2) layer was deposited onto the FTO glass by spin-coating an ethanol solution of titanium isopropoxide (0.5 M) and diethanol amine (0.5 M) at 7000 rpm for 30 s and annealed in air at 500 °C for 2 h. Prior to transferring the substrates into a glove box, the FTO/c-TiO_2 substrates were treated via oxygen plasma for 3 min. Then, $C_4H_{11}N$, $C_6H_{15}N$, and $C_8H_{19}N$ solutions were doped into $CsPbIBr_2$ precursor solutions (in which 367mg $PbBr_2$ and 260mg CsI were dissolved in 1mL DMSO), and precursor solutions with doping ratios of 0.1%, 0.1%, and 0.05% were prepared, respectively. For $CsPbIBr_2$ devices, 90 µL of 1.0 M $CsPbIBr_2$ precursor was spin-coated onto FTO/c-TiO_2 at 1000 rpm for 10 s and 3000 rpm for 50 s, respectively. Particularly, the crystallization process of perovskite thin film included a two-step thermal treatment process. The as-prepared thin film was firstly placed on a hotplate at 30 °C for 1 min and then the temperature was increased to 260 °C for 10 min to remove the remnant solvent and further

improve the crystallization quality of the perovskite thin film. Finally, a carbon back electrode with an average area of 0.09 cm^2 was deposited on a perovskite film using a scraper coating method. Use the same program to manufacture the original device without $CsPbIBr_2$ precursor solutions doped with $C_4H_{11}N$, $C_6H_{15}N$, and $C_8H_{19}N$ solutions.

Characterizations

The morphologies and elemental mapping images were characterized by a scanning electron microscopy (SEM, Hitachi S-4800) The X-ray diffraction (XRD) and depth-dependent grazing incident X-ray diffraction (GIXRD) patterns were recorded by X-ray diffractometer (Bruker D8 Advance). Atomic force microscopy (AFM) characterization was performed on a Bruker ICON2-SYS with a characterization error of 0.256 nm. Kelvin probe force microscopy (KPFM, CypherTM, Asylum Research) was applied to determine the surface potential of the fabricated films. The binding energy spectra were measured by X-ray photoelectron spectroscopy (XPS) spectrometer (Thermo Scientific). Ultraviolet photoelectron spectroscopy (UPS) measurement was performed using He I radiation at 21.2 eV with bias (− 5 V) on the samples to separate the sample and analyzer low-kinetic-energy cutoffs. Ultraviolet–visible (UV–Vis) absorption spectra of various perovskite films were recorded by a Meipuda UV-3200 spectrophotometer in the wavelength range of 450–700 nm. The photocurrent density–voltage (*J-V*) curves of PSCs were recorded on an electrochemical workstation (CHI660E) under irradiation of simulated solar light at optical intensity of 100 mW cm^{-2} (Newport, Oriel Class A, 91195A, AM 1.5G, calibrated by a standard silicon solar cell). The external quantum efficiency (EQE) spectra of various devices were obtained using an IPCE kit from Enli Technology Co., Ltd equipped with a standard Si solar cell as a reference. The opencircuit voltage decay curves were measured at an open-circuit mode by illuminating the device under simulated solar light at optical intensity of 100 mW cm^{-2} for several seconds and then instantaneously switching off the light. The photoluminescence (PL) spectra were recorded via a fluorescence spectrometer excited by a 450 nm laser and the time-resolved photoluminescence (TRPL) decay curves were recorded with a Horiba spectrometer excited by 500 nm laser. To compare phase segregation degree for different films, WITec Alpha 300R Confocal Raman Microscopy was carried out to monitor the PL emission mappings. The Mott-Schottky plots were conducted on an electrochemical workstation (CHI600E, Shanghai Chenhua) at a frequency of 5 kHz with amplitude of 5 mV in the dark.

Statistical Analysis

All statistical analyses were performed with Origin 2022. The data obtained from SEM, UV–vis, PL, TRPL, XPS, XRD, J–V, EIS and EQE were the original data without normalization.The trap state density (N_t) was calculated according to the space-charge-limited current (SCLC) method with the following equation: $N_t = 2\epsilon_0\epsilon_r V_{TFL}/qL^2$,

where V_{TFL} is the onset voltage of the trap-filled limit, q is the elementary charge of an electron, L is the thickness of the perovskite film, and ϵ_0 is the vacuum permittivity and ϵ_r the relative dielectric constant. the Fermi energy level and valence band conduction band were obtained through equation: $WF = E_{max-cut\,off} - 21.2eV$; $VB = WF - E_{min-cut\,off}$; $CB = VB + E_g$. Linear fittings were applied to the dependence of V_{OC} and J_{SC} on the light intensity, and Mott–Schottky plots. Bi-exponential decay function was employed to TRPL decays to explore the carrier transport dynamics. Fifteen PSCs were used to generate the device performance statistics. The summarized champion PCEs for PSCs were gained from reported works.

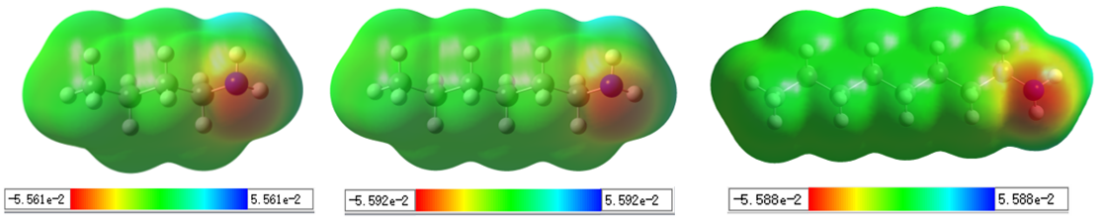

Figure S1. These electrostatic potential images of BA, HA, OA.

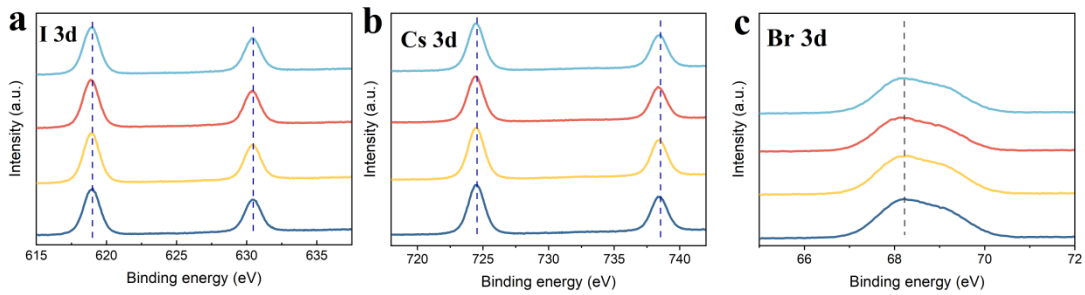

Figure S2. These XPS spectra of (a) I 3d, (b) Cs 3d, and (c) Br 3d control and BA, HA, OA treated perovskite films.

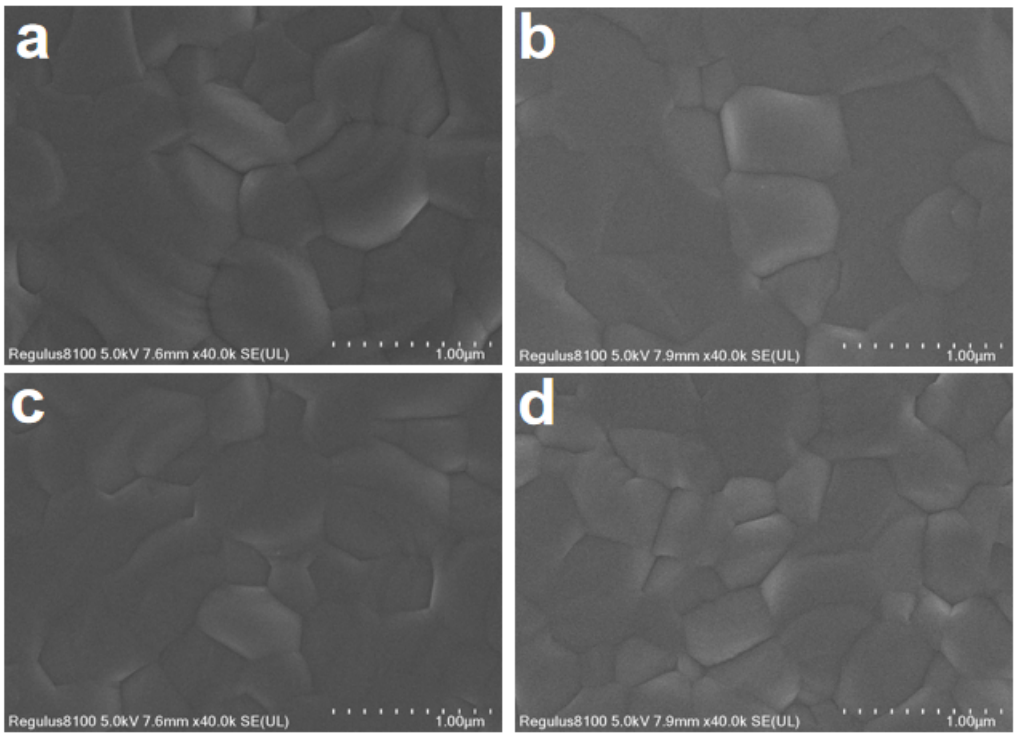

Figure S3. These SEM images of (a) control, (b) BA, (c)HA, and (d) OA treated films.

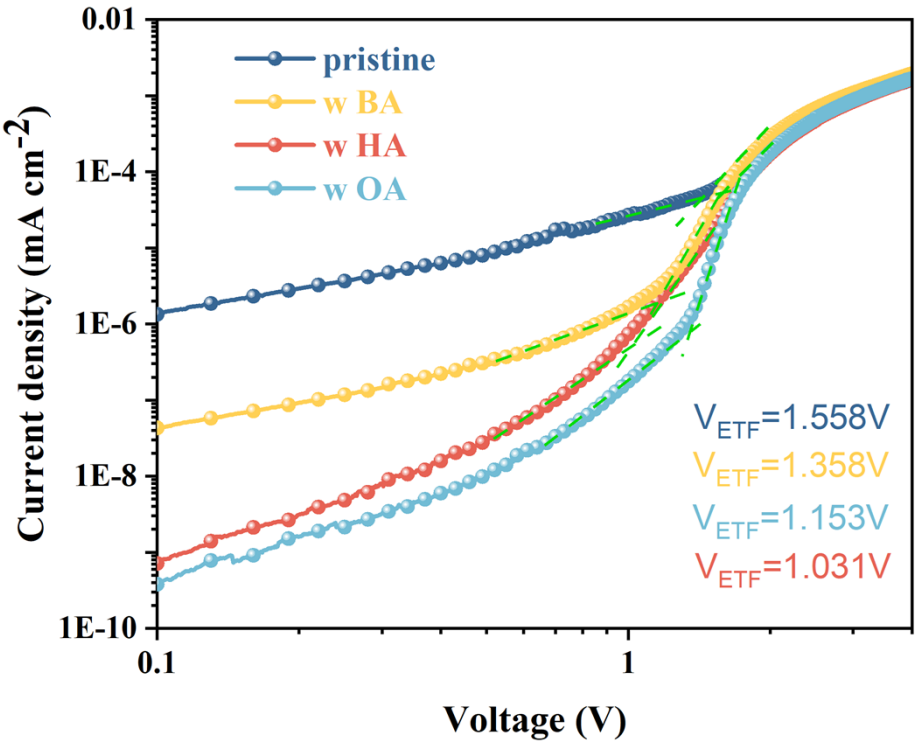

Figure S4. These SCLC curves of control and alkylamine-modified devices.

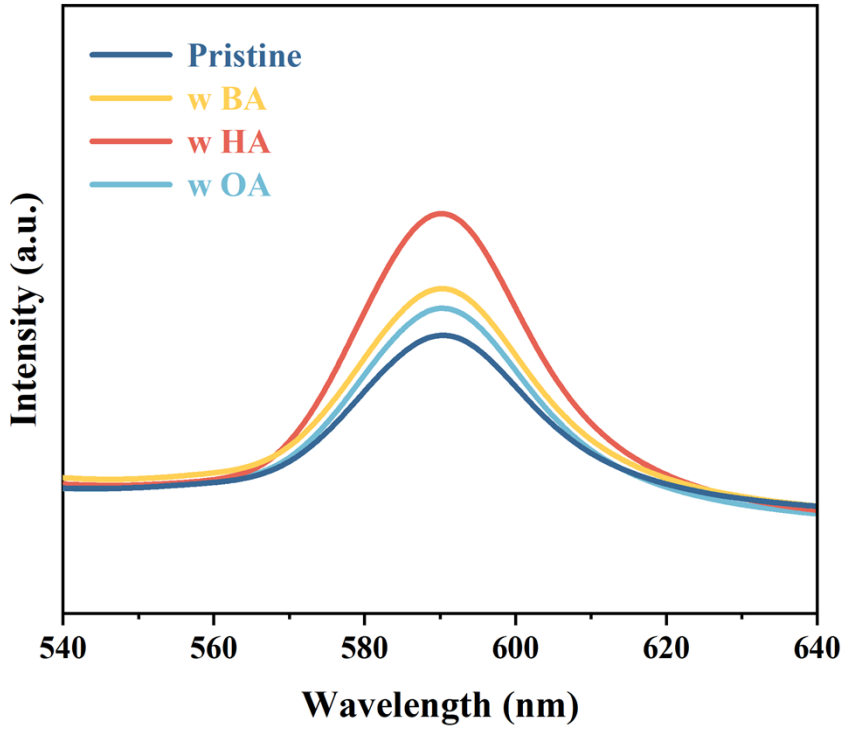

Figure S5. These PL spectra of perovskite films.

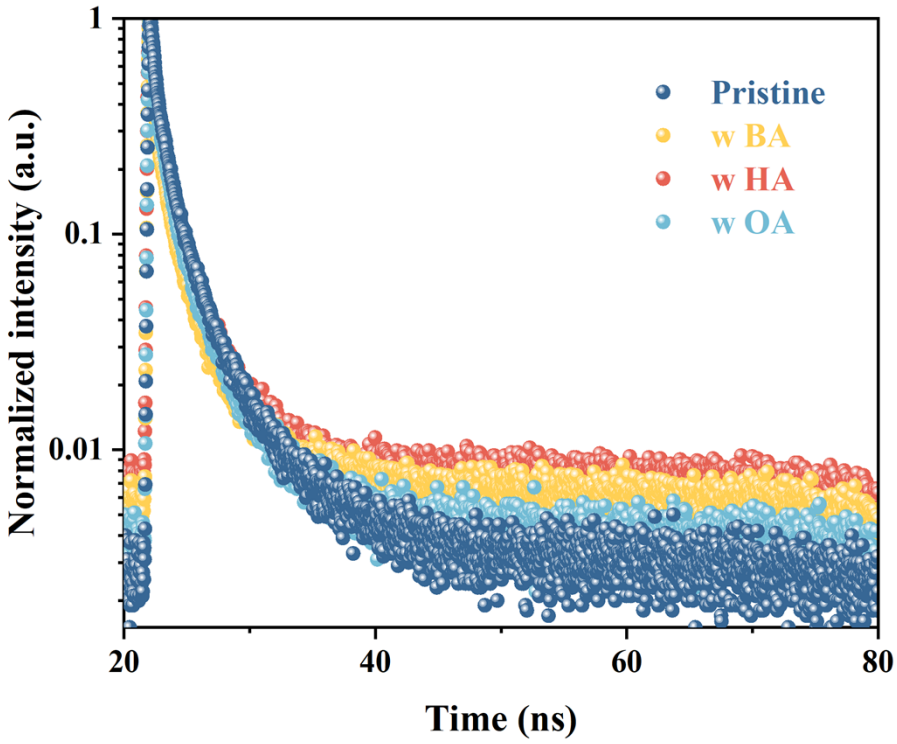

Figure S6. These TRPL spectra of perovskite films.

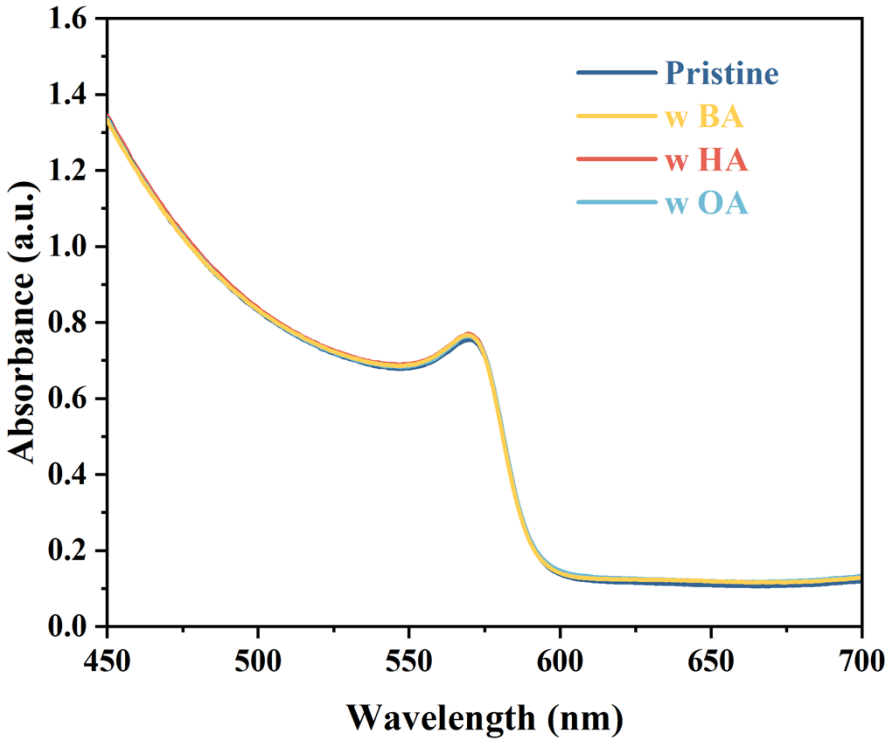

Figure S7. These UV-vis absorption spectra of perovskite films.

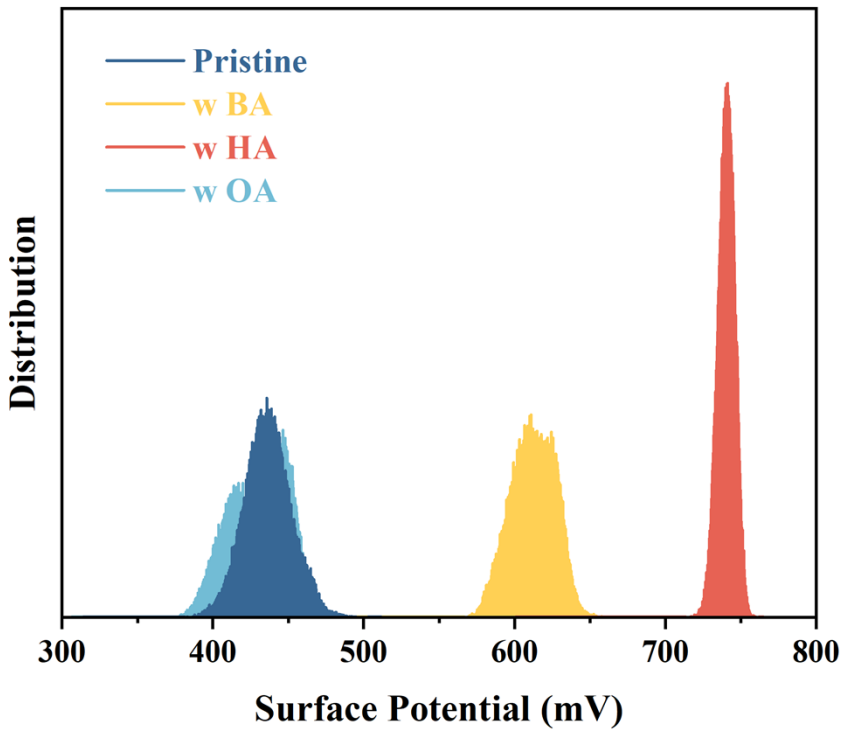

Figure S8. The image of the potential distribution of perovskite films.

Figure S9. These concentration optimization *J*-*V* curves of (a)BA, (b)HA, and (c)OA modified perovskite devices.

Figure S10. (a) PCE, (b)V_{OC},(c) J_{SC} and (d)FF values of $CsPbIBr_2$ perovskite solar cells with different alkylamines.

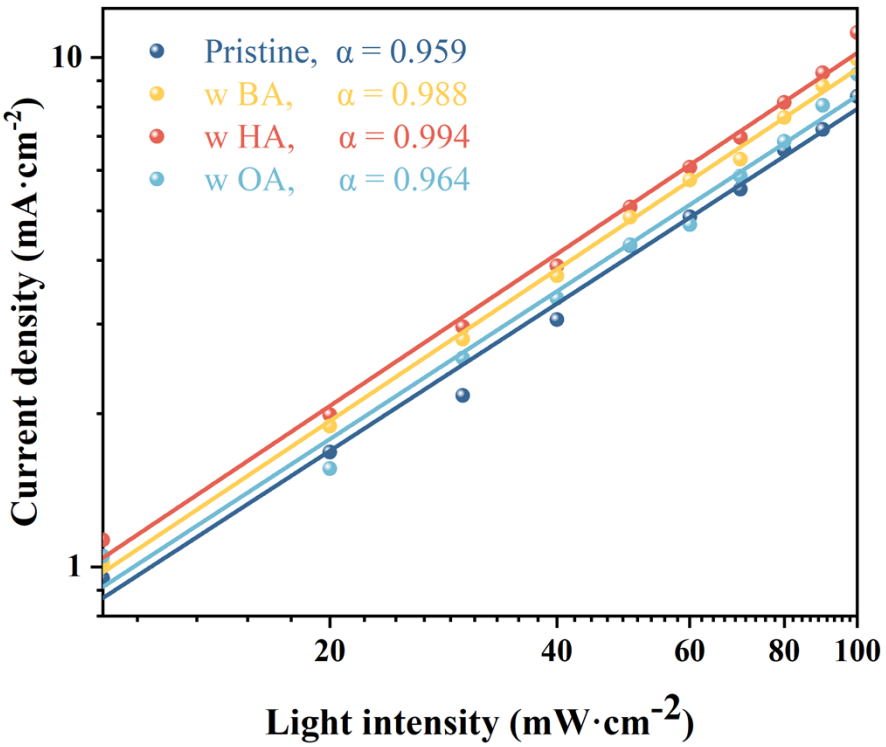

Figure S11. These curves of J_{SC} dependence on light intensity.

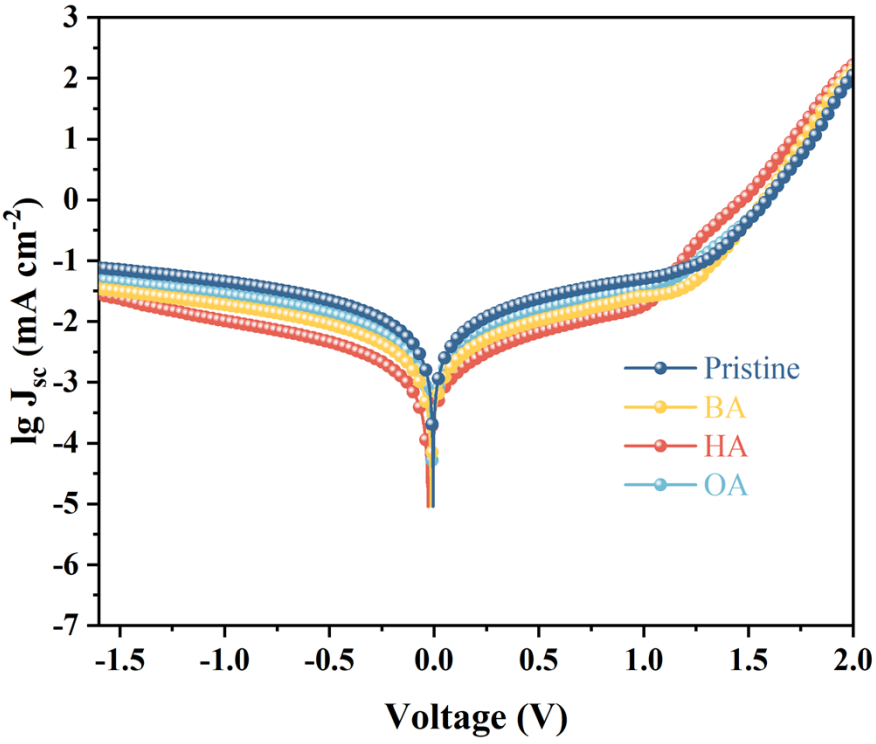

Figure S12. These J-V curves of PSCs in dark.

Figure S13. These (a) open-circuit voltage attenuation curve and (b) carrier lifetime plot of PSCs.

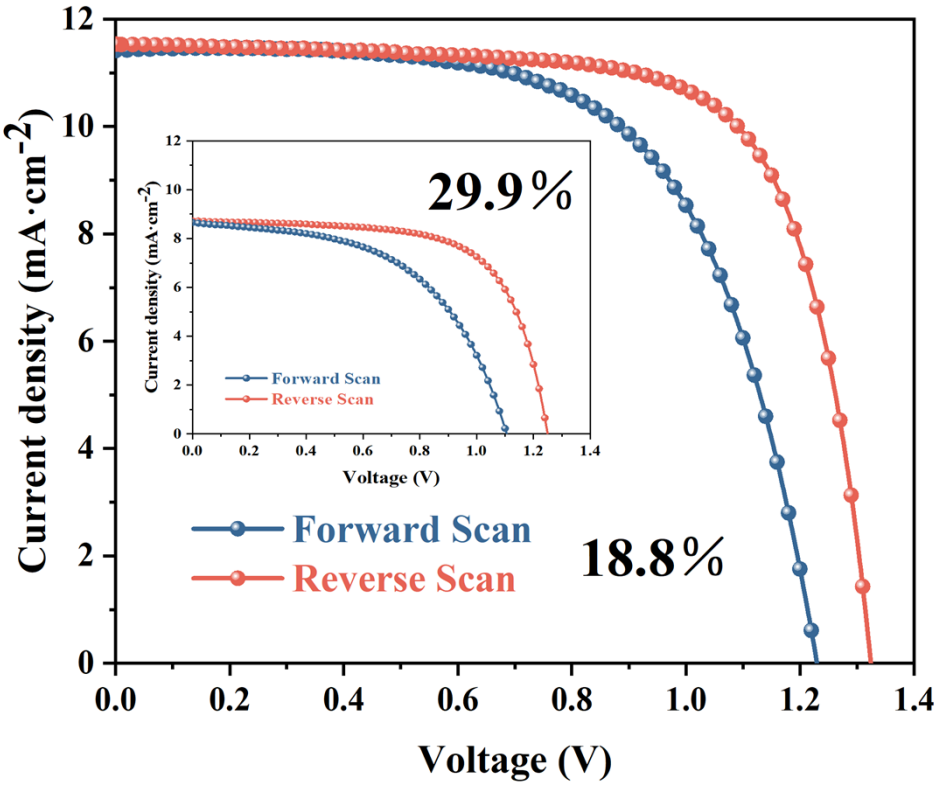

Figure S14. These J–V curves of the champion solar cells measured by forward and reverse scan.

Figure S15. (a) The photovoltaic parameters degradation of control and HA-treated PSCs as a function of storage time under 25 ^{o}C, 5% RH. (b) Thermal stability of PSCs stored at 85 ^{o}C aging.

Table S1. Concentration optimization parameters of perovskites doped with different alkylamines.

Perovskites	Device	J_{SC} (mA cm^{-2})	V_{OC} (V)	FF (%)	PCE (%)
w BA	Pristine	9.894	1.252	68.3	8.46
	0.05%	10.642	1.276	70.3	9.55
	0.10%	10.895	1.297	71.6	10.12
	0.15%	10.229	1.265	69.1	8.94
w HA	Pristine	9.954	1.257	70.9	8.87
	0.05%	10.847	1.288	71.4	9.98
	0.10%	11.254	1.320	71.9	10.68
	0.15%	10.510	1.278	69.9	9.39
w OA	Pristine	9.794	1.238	69.7	8.45
	0.05%	10.236	1.252	70.6	9.05
	0.10%	10.546	1.289	70.2	9.54
	0.15%	10.090	1.253	68.7	8.69

Table S2. Photovoltaic parameters of the champion efficiency of different alkylamine-doped $CsPbIBr_2$ PSCs under standard light.

Perovskites	Device	J_{SC} (mA cm^{-2})	V_{OC} (V)	FF (%)	PCE (%)
$CsPbIBr_2$	Pristine	9.844	1.240	68.2	8.32
	w BA	10.895	1.297	71.5	10.10
	w HA	11.254	1.320	71.9	10.68
	w OA	10.389	1.290	70.6	9.46

Table S3. Summary of the photovoltaic data for previously reported $CsPbIBr_2$, $CsPbI_2Br$ (carbon electrode).

Device architecture	J_{SC} (mA cm^{-2})	V_{OC} (V)	FF (%)	PCE (%)	Ref.
FTO/c-TiO_2/$CsPbIBr_2$/Carbon	11.25	1.32	71.90	10.68	This work
FTO/c-TiO_2/(Rb/Ac) doped $CsPbIBr_2$/Carbon	11.74	1.37	67.00	10.78	1
FTO/c-TiO_2/PMMA-$CsPbIBr_2$/Carbon	11.36	1.307	62.00	9.21	2
FTO/c-TiO_2/$CsPbIBr_2$-FAAc/Spiro-OMeTAD/Au	11.65	1.12	72.39	9.44	3
ITO/c-TiO_2/$CsPbIBr_2$/quinoline sulfate/Carbon	11.53	1.298	69.59	10.41	4
FTO/c-TiO_2/$PbIBr_2$-excess $CsPbIBr_2$/Spiro-OMeTAD/Au	10.50	1.254	71.20	9.37	5
ITO/ZnO/SnO_2/$CsPbIBr_2$/$DAPI_2$/Spiro-OMeTAD/Ag	11.03	1.33	75.20	11.02	6
FTO/c-TiO_2/$CsPbI_{1+x}Br_{2-x}$/Carbon	12.30	1.186	75.00	10.94	7
FTO/TiO_2/CsBr/$CsPbIBr_2$/CsBr/Spiro-OMeTAD/Au	11.76	1.24	71.00	10.33	8
FTO/c-TiO_2/$CsPbIBr_2$/Carbon	11.53	1.323	72.9	11.12	9
FTO/c-TiO_2/$CsPbIBr_2$/$(NiCo)_{1-y}Fe_yO_x$-GO/Carbon	12.03	1.29	70.58	10.95	10
FTO/c-TiO_2/$CsPbIBr_2$/Carbon	11.73	1.338	65.00	10.20	11
FTO/SnO_2/$CsPbIBr_2$-PEI/$CsPbIBr_2$-MA/$CsPbIBr_2$/NiO_x/Ag	13.30	1.25	68.00	11.30	12
FTO/c-TiO_2/$CsPb_{0.99}Zn_{0.01}IBr_2$/Spiro-OMeTAD/Ag	11.92	1.28	69.00	10.51	13
FTO/c-TiO_2/$CsPbIBr_2$/Spiro-OMeTAD/Au	12.03	1.10	65.40	8.65	14
FTO/c-TiO_2/$CsPbIBr_2$-NH_4PF_6/Spiro-OMeTAD/Au	12.11	1.13	74.00	10.10	15
ITO/SnO_2/bulk $CsPbIBr_2$/$CsPbIBr_2$ QDs/Spiro-OMeTAD/Au	9.41	1.22	71.36	8.16	16
FTO/c-TiO_2/$CsPbIBr_2$/BN/Carbon	12.12	1.33	74.60	12.05	17
ITO/Cl-TiO_2/$CsPbIBr_2$/BHJ-2/MoO_3/Al	12.50	1.22	72.66	11.08	18
FTO/TiO_2/$CsPbIBr_2$/PCBM/Ag	11.63	1.25	74.00	10.78	19
FTO/c-TiO_2/ $CsPbIBr_2$/Carbon	11.43	1.327	69.70	10.56	20

FTO/TiO_2/$CsPbIBr_2$/PCBM/Ag	11.58	1.21	69.00	10.48	21
FTO/TiO_2/$CsPbIBr_2$/CuSCN/Carbon	10.43	1.13	62.00	7.30	22
ITO/SnO_2/MgO/$CsPbIB_2$/Spiro-OMeTAD/Ag	11.70	1.36	69.35	11.04	23
ITO/passivated SnO_2/$CsPbIBr_2$/Carbon	8.50	1.23	67.00	7.00	24
FTO/SnO_2/ALD-TiO_2/$CsPbIBr_2$/Carbon	10.91	1.27	66.00	9.31	25
FTO/SnO_2/$CsPbIBr_2$-Br/Spiro-OMeTAD/Au	11.94	1.21	72.50	10.47	26
FTO/TiO_2/$CsPbIBr_2$/Carbon	10.99	1.27	58.00	8.10	27
FTO/c-TiO_2/$CsPbIBr_2$-Cu/Spiro-OMeTAD/Ag	12.80	1.21	67.10	10.40	28
FTO/TiO_2/PEG:$CsPbIBr_2$/Spiro-OMeTAD/Ag	12.25	1.21	74.82	11.10	29
ITO/SnO_2/$CsPbIBr_2$/Spiro-OMeTAD/Ag	11.91	1.27	71.72	10.81	30
ITO/ZnO/$CsPbIBr_2$/ Spiro-OMeTAD/Au	11.34	1.289	75.31	11.01	31
FTO/Cs-NiO_x/N749/$CsPbIBr_2$/PCBM/BCP/Ag	11.49	1.19	69.00	9.49	32
FTO/c-TiO_2/$CsPbIBr_2$/Carbon	11.17	1.28	60.00	8.60	33
FTO/TiO_2/$SmBr_3$/Sm-$CsPbIBr_2$/Spiro-OMeTAD/Au	12.75	1.17	73.00	10.88	34
FTO/c-TiO_2/$CsPbIBr_2$/Carbon	10.66	1.24	69.00	9.16	35
FTO/TiO_2/$CsPbI_2Br$/Carbon	9.55	1.24	60.00	7.10	36
FTO/c-TiO_2/CsBr/$CsPbIBr_2$/Carbon	11.80	1.26	72.00	10.71	37
FTO/c-TiO_2/$CsPbIBr_2$-PEG/Spiro-OMeTAD/Au	8.80	1.28	64.90	7.31	38
FTO/c-TiO_2/$CsPbIBr_2$/Carbon	9.11	1.14	63.00	6.55	39
FTO/c-TiO_2/$CsPbIBr_2$-COF/Carbon	11.95	1.327	72.55	11.50	40
FTO/c-TiO_2/m-TiO_2/$CsPbIBr_2$/Carbon	12.15	0.96	53.00	6.14	41
FTO/SnO_2/$CsPbIBr_2$/$PC_{61}BM$/Ag	11.47	1.335	75.33	11.54	42
FTO/c-TiO_2/$CsPbIBr_2$/Spiro-OMeTAD/Au	9.69	1.23	67.40	8.02	43
FTO/c-TiO_2/mp-TiO_2/$CsPbIBr_2$/Spiro-OMeTAD/Au	7.80	1.13	72.00	6.30	44

FTO/NiO_x/$CsPbIBr_2$/MoO_x/Au	10.56	0.85	62.00	5.52	45
FTO/c-TiO_2/$CsPbIBr_2$/Carbon	8.70	0.96	56.00	4.70	46
FTO/c-TiO_2/$CsPbIBr_2$/Spiro-OMeTAD/Au	12.05	1.23	73.71	10.90	47

References

[1] Y. Guo, F. Zhao, X. Wang, J. Tao, D. Zheng, J. Jiang, Z. Hu, J. Chu, *Sol. Energ. Mat. Sol. C.* **2021**, *221*, 110918.

[2] W. Chai, J. Ma, W. Zhu, D. Chen, H. Xi, J. Zhang, C. Zhang, Y. Hao, *ACS Appl. Mater. Inter.* **2021**, *13*, 2868–2878.

[3] Z. Chen, Q. Wang, Y. Xu, R. Zhou, L. Zhang, Y. Huang, L. Hu, M. Lyu, J. Zhu, *ACS Appl. Mater. Inter.* **2021**, *13*, 24654–24661.

[4] D. Wang, W. Li, X. Liu, G. Li, L. Zhang, R. Li, W. Sun, J. Wu, Z. Lan, *ACS Appl. Energy Mater.* **2021**, *4*, 5747–5755.

[5] W. Li, B. Zhu, M. U. Rothmann, A. Liu, W. Chen, Y. Y. Choo, N. Pai, W. Mao, T. Zhang, Q. Bao, X. Wen, U. Bach, J. Etheridge, Y.-B. Cheng, *Sci. China Mater.* **2021**, *64*, 2655–2666

[6] J. He, Q. Wang, Y. Xu, X. Guo, L. Zhou, J. Su, Z. Lin, J. Zhang, Y. Hao, J. Chang, *Small* 2022, 2205962.

[7] Z. Zhang, D. Chen, W. Zhu, J. Ma, W. Chai, D. Chen, J. Zhang, C. Zhang, Y. Hao, *Sci. China Mater.* **2021**, *64*, 2107–2117.

[8] X. Jiang, W. S. Subhani, K. Wang, H. Wang, L. Duan, M. Du, S. Pang, S. Liu, *ACS Appl. Mater. Inter.* **2021**, *8*, 2001994.

[9] F. Yan, J. Duan, Q. Guo, Q. Zhang, X. Yang, P. Yang, Q. Tang, Sci. China Mater. 2022, 1.

[10] J. Du, J. Duan, X. Yang, Y. Duan, Q. Zhou, Q. Tang, *Angew. Chem. Int. Ed.* **2021**, *60*, 10608–10613.

[11] W. Zhu, Z. Zhang, D. Chen, W. Chai, D. Chen, J. Zhang, C. Zhang, Y. Hao, *Nano-Micro Lett.* **2020**, *12*, 87.

[12] B. Gao, J. Meng, *ACS Appl. Energy Mater.* **2020**, *3*, 8249–8256.

[13] Y. Long, C. Wang, X. Liu, J. Wang, S. Fu, J. Zhang, Z. Hu, Y. Zhu, *J. Mater. Chem. C* **2021**, *9*, 2145–2155.

[14] J. Bian, Y. Wu, W. Bi, L. Liu, X. Su, B. Zhang, *Energ. Fuel.* **2020**, *34*, 11472–11478.

[15] J. Pan, X. Zhang, Y. Zheng, W. Xiang, *Sol. Energ. Mat. Sol. C.* **2021**, *221*, 110878.

[16] Y. Guo, X. Yin, M. Que, J. Zhang, S. Wen, D. Liu, H. Xie, W. Que, *Org. Electron.* **2020**, *86*, 105917.

[17] Q. Guo, J. Duan, J. Zhang, Q. Zhang, Y. Duan, X. Yang, B. He, Y. Zhao, Q. Tang, *Adv. Mater*. 2022, 34, 2202301.

[18] W. Chen, D. Li, S. Chen, S. Liu, Y. Shen, G. Zeng, X. Zhu, E. Zhou, L. Jiang, Y. Li, Y. Li, *Adv. Energy Mater.* **2020**, *10*, 2000851.

[19] C. Zhang, K. Wang, Y. Wang, W. S. Subhani, X. Jiang, S. Wang, H. Bao, L. Liu, L. Wan, S. Liu, *Sol. RRL* **2020**, *4*, 2000254.

[20] F. Yan, P. Yang, J. Li, Q. Guo, Q. Zhang, J. Zhang, Y. Duan, J. Duan, Q. Tang, *Chem. Eng. J*. 2022, 430, 132781.

[21] Z. Zhang, F. He, W. Zhu, D. Chen, W. Chai, D. Chen, H. Xi, J. Zhang, C. Zhang, Y. Hao, *Sustain. Energ. Fuels* **2020**, *4*, 4506–4515.

[22] J. Liu, M. Lei, W. Zhang, G. Wang, *Sustain. Energ. Fuels* **2020**, *4*, 4249–4256.

[23] H. Wang, H. Li, S. Cao, M. Wang, J. Chen, Z. Zang, *Sol. RRL* **2020**, *4*, 2000226.

[24] Z. Guo, S. Teo, Z. Xu, C. Zhang, Y. Kamata, S. Hayase, T. Ma, *J. Mater. Chem. A* **2019**, *7*, 1227–1232.

[25] W. Zhu, W. Chai, Z. Zhang, D. Chen, J. Chang, S. Liu, J. Zhang, C. Zhang, Y. Hao, *Org. Electron.* **2019**, *74*, 103–109.

[26] W. Zhang, J. Xiong, J. Li, W. A. Daoud, *Small* **2020**, *16*, 2001535.

[27] G. Wang, J. Liu, M. Lei, W. Zhang, G. Zhu, *Electrochim. Acta* **2020**, *349*, 136354.

[28] P. Liu, X. Yang, Y. Chen, H. Xiang, W. Wang, R. Ran, W. Zhou, Z. Shao, *ACS Appl. Mater. Inter.* **2020**, *12*, 23984–23994.

[29] Y. You, W. Tian, M. Wang, F. Cao, H. Sun, L. Li, *Adv. Mater. Interfaces* **2020**, *7*, 2000537.

[30] S. Cao, H. Wang, H. Li, J. Chen, Z. Zang, *Chem. Eng. J.* **2020**, *394*, 124903.

[31] J. Huang, S. He, W. Zhang, A. Saparbaev, Y. Wang, Y. Gao, L. Shang, G. Dong, L. Nurumbetova, G. Yue, *Sol. RRL* 2022, 6, 2100839.

[32] S. Yang, L. Wang, L. Gao, J. Cao, Q. Han, F. Yu, Y. Kamata, C. Zhang, M. Fan, G. Wei, T. Ma, *ACS Appl. Mater. Inter.* **2020**, *12*, 13931–13940.

[33] Q. Zhang, W. Zhu, D. Chen, Z. Zhang, Z. Lin, J. Chang, J. Zhang, C. Zhang, Y. Hao,

ACS Appl. Mater. Inter. **2019**, *11*, 2997–3005.

[34] W. S. Subhani, K. Wang, M. Du, X. Wang, S. Liu, *Adv. Energy Mater.* **2019**, *9*, 1803785.

[35] W. Zhu, Q. Zhang, D. Chen, Z. Zhang, Z. Lin, J. Chang, J. Zhang, C. Zhang, Y. Hao, *Adv. Energy Mater.* **2018**, *8*, 1802080.

[36] Y. Guo, F. Zhao, Z. Li, J. Tao, D. Zheng, J. Jiang, J. Chu, *Org. Electron.* **2020**, *83*, 105731.

[37] W. Zhu, Z. Zhang, W. Chai, Q. Zhang, D. Chen, Z. Lin, J. Chang, J. Zhang, C. Zhang, Y. Hao, *ChemSusChem* **2019**, *12*, 2318–2325.

[38] J. Lu, S.-C. Chen, Q. Zheng, *ACS Appl. Energy Mater.* **2018**, *1*, 5872–5878.

[39] W. Zhu, Q. Zhang, C. Zhang, Z. Zhang, D. Chen, Z. Lin, J. Chang, J. Zhang, Y. Hao, *ACS Appl. Energy Mater.* **2018**, *1*, 4991–4997.

[40] J. Zhang, J. Duan, Q. Guo, Q. Zhang, Y. Zhao, H. Huang, Y. Duan, Q. Tang, *ACS Energy Lett*. 2022, 7, 3467-3475.

[41] J. Liang, Z. Liu, L. Qiu, Z. Hawash, L. Meng, Z. Wu, Y. Jiang, L. K. Ono, Y. Qi, *Adv. Energy Mater.* **2018**, *8*, 1800504.

[42] H. Xiao, C. Zuo, L. Zhang, W. Zhang, F. Hao, C. Yi, F. Liu, H. Jin, L. Ding, *Nano Energy* 2022, 106, 108061.

[43] W. Li, M. U. Rothmann, A. Liu, Z. Wang, Y. Zhang, A. R. Pascoe, J. Lu, L. Jiang, Y. Chen, F. Huang, Y. Peng, Q. Bao, J. Etheridge, U. Bach, Y.-B. Cheng, *Adv. Energy Mater.* **2017**, *7*, 1700946.

[44] Q. Ma, S. Huang, X. Wen, M. A. Green, A. W. Y. Ho-Baillie, *Adv. Energy Mater.* **2016**, *6*, 1502202.

[45] C. Liu, W. Li, J. Chen, J. Fan, Y. Mai, R. E. I. Schropp, *Nano Energy* **2017**, *41*, 75–83.

[46] C. F. J. Lau, X. Deng, Q. Ma, J. Zheng, J. S. Yun, M. A. Green, S. Huang, A. W. Y. Ho-Baillie, *ACS Energy Lett.* **2016**, *1*, 573–577.

[47] Q. Wang, Y. Xu, L. Zhang, A. Yang, T. Bai, F. Liu, M. Lyu, J. Zhu, *ACS Appl. Energy Mater*. **2022**, 5, 3110–3118.